Long-Range Reactive Dynamics in Myoglobin

J. Timothy Sage,[1,*] Stephen M. Durbin,[2] Wolfgang Sturhahn,[3] David C. Wharton,[1] Paul M. Champion,[1] Philip Hession,[2,3] John Sutter,[2,3] and E. Ercan Alp[3]

[1]*Department of Physics and Center for Interdisciplinary Research on Complex Systems, Northeastern University, Boston, Massachusetts 02115*

[2]*Department of Physics, Purdue University, West Lafayette, Indiana 47907*

[3]*Advanced Photon Source, Argonne National Laboratory, Argonne, Illinois 60439*

(Received 30 August 1999)

We report the complete vibrational spectrum of the probe nucleus ^{57}Fe at the oxygen-binding site of the protein myoglobin. The Fe-pyrrole nitrogen stretching modes of the heme group, identified here, probe asymmetric interactions with the protein environment. Collective oscillations of the polypeptide, rather than localized heme vibrations, dominate the low frequency region. We conclude that the heme "doming" mode is significantly delocalized, so that distant sites respond to oxygen binding on vibrational time scales. This has ramifications for understanding long-range interactions in biomolecules, such as those that mediate cooperativity in allosteric proteins.

DOI: 10.1103/PhysRevLett.86.4966 PACS numbers: 87.15.He, 36.20.Ng, 87.64.Pj

Heme proteins are exemplary systems for investigating the influence of protein dynamics on physiological function [1,2]. Although the Fe atom at the center of the planar heme group is ordinarily the site of reaction, the dynamics of the surrounding protein matrix control access to and reactivity of the heme. In the case of the oxygen-binding protein myoglobin (Mb), low frequency vibrations directly couple to the binding of diatomic ligands to Fe [3,4]. A recent report of far infrared *emission* following visible excitation of Mb [5] may be a related phenomenon.

However, the character of these reactive low frequency modes remains elusive. The most apparent structural change upon ligand release from Mb is a localized "doming" of the heme at the oxygen-binding site, which involves Fe motion out of the mean heme plane and an associated distortion of the heme from planarity [6]. On the other hand, transient grating experiments [7] indicate a prompt collective response of the entire protein to ligand dissociation. This issue has crucial implications for understanding the nature and time scale of interactions among spatially separated sites, as exemplified by cooperative O_2 binding to multiple heme sites in hemoglobin [8].

In this Letter, we employ nuclear resonance vibrational spectroscopy (NRVS) to determine the complete vibrational frequency spectrum of the probe nucleus ^{57}Fe, located at the active site of Mb. Exploiting the recoil energy associated with absorption of an x-ray photon, NRVS detects vibrational sidebands at energies above (below) a nuclear resonance, which correspond to the creation (annihilation) of a vibrational quantum coincident with the excitation of the nucleus. In contrast with conventional Mössbauer spectroscopy, where measurements of the recoilless nuclear resonant absorption yield the total mean square fluctuations $\langle x_{\mathrm{Fe}}^2 \rangle$ of the heme Fe [2,9,10], NRVS provides a direct measure of the mean square displacement of the ^{57}Fe nucleus *at each frequency* [11]. Quantitative analysis of these spectra allows us to identify the previously unobserved Fe-pyrrole stretching frequencies and establish their sensitivity to the local environment of the heme. Heme doming does not contribute the spectral intensity predicted for an isolated heme, demonstrating that this mode is delocalized in the protein environment.

Techniques for high-resolution NRVS have been described [12,13]. Perfect crystal optics produce an x-ray beam tunable through the $E_0 = 14.413$ keV ^{57}Fe nuclear resonance energy with 0.85 meV resolution [14]. The x-ray energy is scanned so that $E - E_0$ covers the relevant range of vibrational energies. Atomic Fe K fluorescence, which follows deexcitation of the nucleus, is monitored to determine the excitation probability at each energy. Measurements were performed at sector 3-ID of SRI-CAT at the Advanced Photon Source, Argonne National Laboratory. Spectra were recorded from samples mounted in a cryostat and exposed to a 0.7 GHz photon flux in a 0.5×2 mm^2 beam.

Established methods [15] were used to remove the heme from horse heart Mb and replace it with heme enriched to 93.6% in ^{57}Fe. Buffered Mb solutions were concentrated to 13 mM, reduced with sodium dithionite to produce the deoxygenated protein (deoxyMb), and exposed to CO gas to produce the CO complex (MbCO). For photolysis measurements, 9 mM MbCO in 75% glycerol was loaded into a channel milled in a sapphire block. Spectra of photolyzed MbCO were recorded under continuous illumination with a 15 mW HeNe laser beam ($\lambda = 632.8$ nm) directed onto the sample through a fiber optic cable.

NRVS data recorded on frozen solutions of deoxyMb and MbCO (Fig. 1) reveal numerous vibrational features. A broad feature near 250 cm^{-1}, previously observed at 4.4 meV resolution [13], dominates the high frequency region of the deoxyMb spectrum. In deoxyMb, the oxygen-binding site is vacant and the remaining Fe neighbors are the four pyrrole nitrogen atoms of the heme and the nitrogen of histidine-93. The Fe-His bond is the only

 0031-9007/01/86(21)/4966(4)$15.00

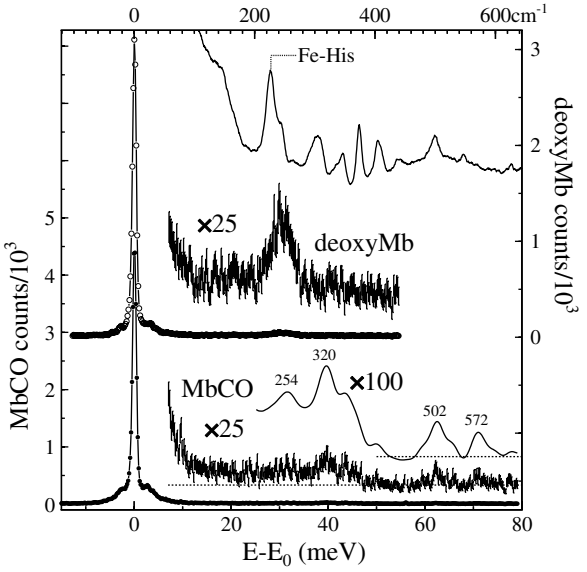

FIG. 1. NRVS data recorded from frozen solutions of ^{57}Fe-enriched MbCO (solid circles) at 110 ± 5 K and deoxyMb (open circles) at 35–70 K. Temperatures were estimated from the relative intensity of phonon creation and annihilation peaks. The MbCO (deoxyMb) spectrum is the sum of 20(16) independent scans sampled every 0.2 meV over an energy range extending from −15 meV to 80(55) meV with a total accumulation time of 189(160) sec/channel. The high frequency region of the MbCO spectrum is scaled up by an additional factor of 4, subjected to an 11-point smooth, and displayed as a solid curve. The solid curve at the top of the figure is the resonance Raman spectrum of deoxyMb at 100 K.

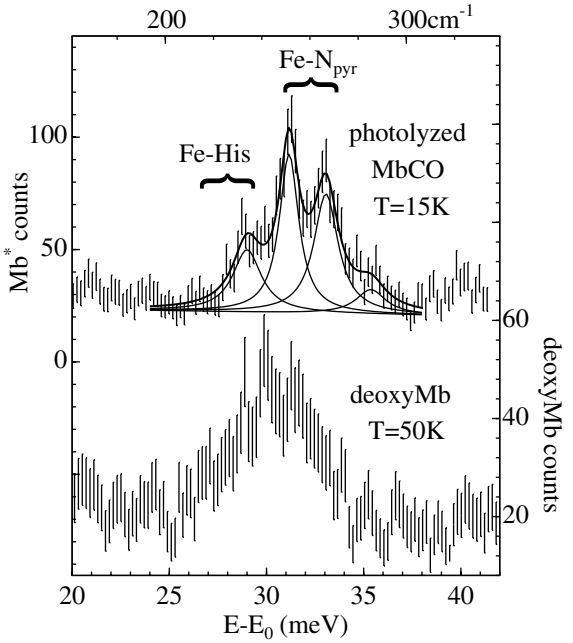

FIG. 2. Comparison of the 250 cm^{-1} mode clusters of deoxyMb and Mb*. The Mb* data were recorded under continuous illumination. The temperature of a sensor mounted in the sapphire sample block was 15 K.

covalent bond between the heme and the protein. The Fe-His stretching frequency has been identified in low temperature resonance Raman spectra [16] at 227 cm^{-1}, and is clearly only a minor component of the 250 cm^{-1} feature. CO binding to Fe significantly reduces the NRVS intensity in the 250 cm^{-1} region, but the MbCO spectrum includes features at 502 and 572 cm^{-1}, corresponding to Fe-C stretching and Fe-C-O bending frequencies previously identified using resonance Raman spectroscopy [17]. Additional features of the MbCO spectrum appear at 254 and 320 cm^{-1}.

Illumination of MbCO efficiently photolyzes the Fe-CO bond. Spectra of photolyzed MbCO (Mb*) resemble deoxyMb, but improved statistics allow individual components of the 250 cm^{-1} feature to be clearly resolved (Fig. 2). The lowest energy component resulting from a least-squares fit to a series of Lorentzians (Table I) appears at 234 cm^{-1} in Mb*, consistent with previous low temperature observations of the Fe-His frequency [16]. The dominant components in Mb* appear at 251 and 267 cm^{-1}.

A more detailed characterization of the modes contributing to the 250 cm^{-1} cluster results from quantitative analysis. The delayed 6.4 keV fluorescence signal emitted from a given excitation volume is proportional to the absorption cross section [18] $\sigma(E) = \frac{\pi}{2}\Gamma_n\sigma_0 S(E - E_0)$, where σ_0 is the nuclear cross section and Γ_n is the linewidth of the recoilless resonance. The excitation probability per unit energy

$$S(E) = \sum_{if} p_i |\langle f|e^{i\vec{k}\cdot\vec{r}_{\mathrm{Fe}}}|i\rangle|^2 \mathcal{L}[E - (E_f - E_i)] \quad (1)$$

includes vibrational features displaced from the recoilless ($E_i = E_f$) nuclear resonance at E_0 by the energy difference between initial and final vibrational states $|i\rangle$ and $|f\rangle$. Fluctuations in the position $\vec{r}_{\mathrm{Fe}}$ of the Fe atom determine the strength of the vibrational features through the matrix element $\langle f|e^{i\vec{k}\cdot\vec{r}_{\mathrm{Fe}}}|i\rangle$. In Eq. (1), $\vec{k}$ is the incident photon wave vector and p_i is the population of the initial vibrational state. Since the line-shape function $\mathcal{L}[E]$ has unit area, $\int S(E)\,dE = 1$ by closure, and the integrated cross section is a constant independent of the Fe environment [19].

TABLE I. Frequencies, mode composition, and assignments for observed vibrational features.

	Frequency (cm^{-1})	e^2_{Fe}	Mode assignment
MbCO	502	0.45	Fe-CO stretch
	572	0.16	Fe-C-O bend
Mb*	234	0.25	Fe-His stretch
	251	0.48	Fe-N_{pyr} stretch
	267	0.48	Fe-N_{pyr} stretch
	285	0.13	···

For a normal mode Q of frequency ω expressed in terms of mass-weighted atomic coordinates as $Q = \sum_j \sqrt{m_j}\,\vec{r}_j \cdot \vec{e}_j$, the feature due to one-phonon transitions $|n\rangle \rightarrow |n+1\rangle$ appearing at energy $E_0 + \hbar\omega$ constitutes a fraction [20]

$$\phi = \langle(\vec{e}_{\mathrm{Fe}} \cdot \hat{k})^2\rangle \frac{E_R}{\hbar\omega}(\bar{n}+1)f \qquad (2)$$

of the integrated cross section that depends on the average vibrational excitation $\bar{n} = [\exp(\hbar\omega/k_BT) - 1]^{-1}$ of the mode at temperature T. Equation (2) is valid in the limit $\hbar\omega/\sqrt{\bar{n}(\bar{n}+1)} > e^2_{\mathrm{Fe}}E_R$, where $E_R = \hbar^2k^2/2m_{\mathrm{Fe}} = 1.96$ meV is the ^{57}Fe recoil energy. For a randomly oriented sample such as the solutions studied here, the angular average yields $\langle(\vec{e}_{\mathrm{Fe}} \cdot \hat{k})^2\rangle = \frac{1}{3}e^2_{\mathrm{Fe}}$. The recoilless fraction $f = \exp(-k^2\langle x^2_{\mathrm{Fe}}\rangle)$ reflects the decreased area of the central resonance due to the total rms Fe fluctuations along the beam direction and ensures spectral normalization.

The Fe mode composition factor e^2_{Fe} is equal to the fraction of kinetic energy invested in Fe motion, and provides direct information on mode character. For selected discrete NRVS peaks, we determined area fractions ϕ, normalized according to Ref. [12]. Inversion of Eq. (2), using reported recoilless fractions [21], then yields e^2_{Fe} values listed in Table I for Mb* and MbCO. Since the Fe-C-O bending mode is expected to have two nearly degenerate components, the value reported in Table I for the 572 cm^{-1} feature is half the value determined from the spectral area. The values reported for Mb* assume complete photolysis of the sample. The 1.7 cm^{-1} ^{54}Fe/^{57}Fe frequency shift reported [22] for the Fe-His mode in deoxyMb yields $e^2_{\mathrm{Fe}} \cong -2d(\ln\omega)/d(\ln m_{\mathrm{Fe}}) = 0.29$ for the Fe-His mode, in reasonable agreement with the value (0.25) determined here for Mb*.

Straightforward reasoning based on the results listed in Table I yields strong conclusions about the geometry of Fe motion contributing to the mode cluster in Fig. 2. Summation over all normal modes yields $\Sigma(\vec{e}_{\mathrm{Fe}} \cdot \hat{u})^2 = 1$ for any direction $\hat{u}$. Since $\Sigma e^2_{\mathrm{Fe}} > 1$ for the Mb* modes listed in Table I, Fe motion cannot occur in the same direction for all these modes. Moreover, placement of the Fe on an axis of near fourfold symmetry restricts observed features either to modes involving out-of-plane Fe motion or to quasidegenerate pairs of modes involving orthogonal in-plane Fe motion. As a result, we must attribute the pair of Mb* bands observed at 251 and 267 cm^{-1} to a quasidegenerate pair of in-plane Fe modes. This conclusion agrees well with recent calculations on heme model systems [23], which predict that a pair of Fe-pyrrole nitrogen (Fe-N_{pyr}) stretching modes (ν_{53}) at 251 and 266 cm^{-1} dominate in-plane Fe motion.

The protein perturbs the approximately fourfold symmetric environment of the heme Fe and lifts the nominal x-y degeneracy of the Fe-N_{pyr} frequencies. Specific structural features likely to contribute to the Fe-N_{pyr} frequency separation include the binding of His-93 to the heme Fe and the 9°–12° tilt of pyrrole ring C from the mean heme plane, visible in crystal structures of Mb [6,24].

In addition to discrete peaks, Fig. 1 reveals an underlying vibrational continuum, visible to nearly 400 cm^{-1} in MbCO. This component of the NRVS signal increases below 100 cm^{-1}, culminating in a shoulder on the recoilless resonance (Fig. 3). As the temperature increases, the shoulder resolves into a broad peak near 25 cm^{-1}, similar to features observed in inelastic neutron scattering from hydrated protein films [5,25] and in site-selected fluorescence spectra of Zn-substituted Mb [26]. Calculated normal modes of the protein in this frequency region involve torsional oscillations of the polypeptide backbone and side chains [27]. Translation of the entire heme in response to these collective oscillations dominates the observed frequency spectrum of Fe fluctuations (Fig. 1), as predicted for Mb [28].

Although NRVS provides *site-selective* access to the low frequency regime, additional sharp features attributable to localized heme vibrations are not apparent in Fig. 3. This is unexpected, since the doming frequency of an isolated heme is predicted [23] to appear at 50–70 cm^{-1}. Moreover, structural changes upon CO binding to Mb [6] implicate heme doming as a significant component of oscillations coupled to ligand dissociation from MbNO

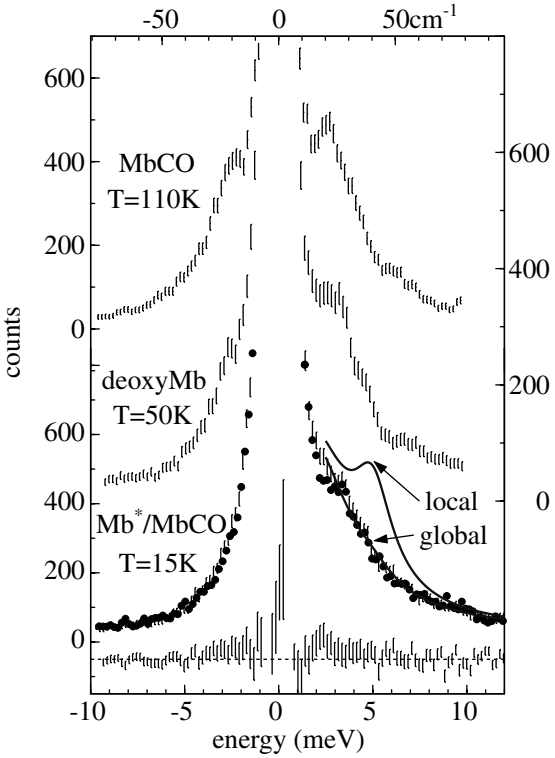

FIG. 3. Low frequency spectra of MbCO, deoxyMb, and Mb*. Filled circles overlaid on the Mb* spectrum represent the spectrum of unphotolyzed MbCO at 15 K, and the Mb*-MbCO difference signal appears at the bottom of the figure. Solid curves represent predictions described in the text.

and MbCO observed [4] at 40 and 80 cm^{-1}. Differences between the MbCO and deoxyMb NRVS signals in this frequency region are negligible (Fig. 3, bottom), underscoring the absence of the expected ligation-sensitive doming resonance and suggesting that the doming mode acquires a nonlocal character in the protein through vibrational mixing with the collective oscillations (i.e., involvement of many atoms reduces e^2_{Fe}).

Quantitative analysis of two simple limiting cases supports this conclusion. To estimate the expected contribution of local heme doming analogous to the model calculation [23], we consider motion of the Fe and the imidazole ring of the histidine ($m_1 = 122$) as a rigid body against the porphyrin skeleton ($m_2 = 300$) of the heme group. The spectral contribution predicted for such a local oscillation at 40 cm^{-1}, using the value $e^2_{\mathrm{Fe}} = (m_{\mathrm{Fe}}/m_1)m_2/(m_1 + m_2) = 0.33$ in Eq. (2), would be clearly evident above the collective mode background, as indicated by the solid curve in Fig. 3.

To illustrate the opposite extreme, we increase the masses in the effective two-body oscillator to include the entire F-helix ($m_1 = 1002$, including the heme Fe and residues 86-94) and the E-helix ($m_2 = 2374$, including the porphyrin skeleton and residues 58-77), motivated by the "scissoring" motion of the E- and F-helices upon CO binding recently identified in ultrahigh resolution x-ray structures [24]. In this limit, the predicted Fe fluctuations decrease by nearly an order of magnitude and are too small to resolve from the collective mode background (Fig. 3). This global motion thus accounts for the absence of a clearly resolved doming resonance in the NRVS signal.

NRVS provides insights into active site structure and dynamics that are not available from other methods. Quantitative analysis, coupled with the absence of selection rules, enables identification of the Fe-N_{pyr} frequencies, which monitor asymmetric interactions with the protein environment. Moreover, site-selective access to the low frequency regime quantifies the extent to which reactive dynamics are localized at the Fe. The delocalization of heme doming deduced from NRVS has important ramifications: (1) in this new experimental regime, realistic models for vibrational dynamics must include the polypeptide and (2) the active site communicates with distant sites on vibrational time scales (e.g., 8.0 ps for a 40 cm^{-1} mode).

We thank T. S. Toellner and M. Y. Hu for support during experiments. V. Šrajer and W. M. Reiff provided valuable assistance in sample characterization. We acknowledge financial support from NIH GM-52002 (J. T. S.), NIH DK-35090 (P. M. C.), NSF 99-83100 and 99-04516 (J. T. S. and P. M. C.), and DOE DE-F602-96-ER45581A (S. M. D.). Use of the Advanced Photon Source was supported by the U.S. Department of Energy, Basic Energy Sciences, Office of Science, under Contract No. W-31-109-Eng-38.

*Electronic address: jtsage@neu.edu

[1] J. T. Sage and P. M. Champion, in *Small Substrate Recognition in Heme Proteins, Comprehensive Supramolecular Chemistry,* edited by K. S. Suslick (Pergamon, Oxford, U.K., 1996), Chap. 6, pp. 177–218.
[2] H. Frauenfelder, F. Parak, and R. D. Young, Annu. Rev. Biophys. Biophys. Chem. **17**, 451 (1988).
[3] R. H. Austin, M. W. Roberson, and P. Mansky, Phys. Rev. Lett. **62**, 1912 (1989).
[4] L. Zhu, J. T. Sage, and P. M. Champion, Science **226**, 629 (1994); P. M. Champion *et al.,* Proc. SPIE Int. Soc. Opt. Eng. **3273**, 80 (1998); F. Rosca *et al.,* J. Phys. Chem. A **104**, 4280 (2000).
[5] H. Leyser, W. Doster, and M. Diehl, Phys. Rev. Lett. **82**, 2987 (1999).
[6] J. Kuriyan, S. Wilz, M. Karplus, and G. A. Petsko, J. Mol. Biol. **192**, 133 (1986).
[7] L. Genberg, L. Richard, G. McLendon, and R. J. D. Miller, Science **251**, 1051 (1991).
[8] R. E. Dickerson and I. Geis, *Hemoglobin: Structure, Function, Evolution, and Pathology* (Benjamin/Cummings, Menlo Park, CA, 1983).
[9] H. Keller and P. G. Debrunner, Phys. Rev. Lett. **45**, 68 (1980).
[10] F. Parak and E. W. Knapp, Proc. Natl. Acad. Sci. U.S.A. **81**, 7088 (1984).
[11] H. Paulsen *et al.,* Phys. Rev. B **59**, 975 (1999).
[12] W. Sturhahn *et al.,* Phys. Rev. Lett. **74**, 3832 (1995).
[13] C. Keppler *et al.,* Eur. Biophys. J. **25**, 221 (1997).
[14] T. S. Toellner *et al.,* Appl. Phys. Lett. **71**, 2112 (1997).
[15] F. W. J. Teale, Biochim. Biophys. Acta **35**, 543 (1959).
[16] D. L. Rousseau and J. M. Friedman, in *Biological Applications of Raman Spectroscopy,* edited by T. G. Spiro (Wiley-Interscience, New York, 1988), Vol. 3, pp. 133–215.
[17] E. Kerr and N.-T. Yu, in *Biological Applications of Raman Spectroscopy,* edited by T. G. Spiro (Wiley-Interscience, New York, 1988), Vol. 3, pp. 39–95.
[18] K. S. Singwi and A. Sjölander, Phys. Rev. **120**, 1093 (1960).
[19] H. J. Lipkin, Phys. Rev. B **52**, 10 073 (1995).
[20] W. Sturhahn and V. G. Kohn, Hyperfine Interact. **123/124**, 367 (2000); A. C. Zemach and R. J. Glauber, Phys. Rev. **101**, 118 (1956).
[21] I. Chang *et al.,* Chem. Phys. **212**, 221 (1996); L. Cordone *et al.,* Eur. Biophys. J. **27**, 173 (1998).
[22] P. V. Argade *et al.,* J. Am. Chem. Soc. **106**, 6593 (1984).
[23] P. M. Kozlowski, T. G. Spiro, A. Bérces, and M. Z. Zgierski, J. Phys. Chem. B **102**, 2603 (1998); P. M. Kozlowski, T. G. Spiro, and M. Z. Zgierski, J. Phys. Chem. B **104**, 10 659 (2000).
[24] G. S. Kachalova, A. N. Popov, and H. D. Bartunik, Science **284**, 473 (1999).
[25] W. Doster, S. Cusack, and W. Petry, Nature (London) **337**, 754 (1989); J. C. Smith, Q. Rev. Biophys. **24**, 227 (1991).
[26] J. S. Ahn, Y. Kanematsu, M. Enomoto, and T. Kushida, Chem. Phys. Lett. **215**, 336 (1993).
[27] Y. Seno and N. Go, J. Mol. Biol. **216**, 95 (1990).
[28] B. Melchers *et al.,* Biophys. J. **70**, 2092 (1996).